Journal of Magnetism and Magnetic Materials 424 (2017) 410–415

Contents lists available at ScienceDirect

Journal of Magnetism and Magnetic Materials

journal homepage: www.elsevier.com/locate/jmmm

Fabrication, morphological, structural and magnetic properties of electrodeposited Fe_3Pt nanowires and nanotubes

U. Khan[a], N. Adeela[b], Wenjing Li[a], M. Irfan[a], K. Javed[a], S. Riaz[a], X.F. Han[a,*]

[a] Beijing National Laboratory for Condensed Matter Physics, Institute of Physics, Chinese Academy of Sciences, Beijing 100190, China
[b] Centre for High Energy Physics, University of the Punjab, Lahore 54000, Pakistan

ARTICLE INFO

Keywords:
Fe_3Pt NWs and NTs
Electrodeposition
Magnetic field (MF) annealing

ABSTRACT

Highly ordered Fe_3Pt nanowires (NWs) and nanotubes (NTs) embedded in anodic aluminum oxide (AAO) template have been fabricated by dc electrodeposition method. Response of heat treatment on structural and magnetic properties of the samples has been studied with and without the presence of magnetic field (1 T). X-Ray Diffraction analysis shows chemically ordered $L1_2$ face centered cubic (FCC) as the dominant phase for Fe_3Pt NWs and heat treatment improves crystallinity with retained its phase. Whereas, Fe_3Pt NTs show amorphous behavior with and without magnetic field annealing. Furthermore, magnetic properties of the samples have been investigated by vibrating sample magnetometer (VSM). Magnetic parameters of Fe_3Pt including magnetic coercivity, saturation magnetization, squareness and shape of MH-loops have been investigated as a result of simple and MF annealing.

1. Background

Magnetic nanostructures have attracted a great deal of attention during the last decade because of their prospective applications not only in micro-electromechanical systems (MEMS), sensors, and high density recording media but also in functional micro and nanodevices [1–4]. For such applications both soft and hard magnetic materials are required [5]. In addition, reduction in size can lead to both quantitative and qualitative changes in several magnetic and transport properties in comparison with bulk [6–11].

Among several binary systems, Fe-Pt system has gained much attention and scientists are investigating its magnetic properties due to the presence of three different superlattice structures [12]. One is FePt denoted with its strukturbericht symbol as $L1_0$ and this structure includes extremely large perpendicular magnetic anisotropy which is highly demanded for magnetic storage devices. The rest of two structures include $FePt_3$ and Fe_3Pt which are structurally represented as $L1_2$ phase. Fe_3Pt is an important candidate which has already been prepared with physical and chemical fabrication routes [13–15] and is being used a host of several properties due to its interesting magnetic characteristics, like invar effect, martensitic transformations, shape memory effects and giant magnetostriction [16–19]. Fe_3Pt with $L1_2$ structural phase demonstrates small perpendicular magnetic anisotropy in both its disordered and ordered phases due to cubic symmetry. However, there are few reports on 1D Fe_3Pt nanowires (NWs) and nanotubes (NTs) and little attention has been given to its magnetic properties after heat treatment.

Previously, post annealing effects of metals, binary alloys and multilayer nanostructures have been investigated [20–26]. In addition, it has been noticed that magnetic properties of materials can be considerably enhanced by heat treatment in the presence of magnetic field [20,21]. The motivation behind this work is to investigate annealing impact on Fe_3Pt NWs and NTs embedded in anodic aluminum oxide (AAO) template and compare structural and magnetic properties of these nanostructures with and without magnetic field (MF) annealing.

2. Experimental section

A polycrystalline Fe_3Pt NWs and amorphous NTs were prepared by DC electrodeposition method. In this synthesis process, mechanical properties, chemical stability, and inter-pore distances of AAO templates are characteristic features [27]. High purity aluminum (Al) foil with thickness of 5 cm x 3 cm x 0.5 mm was utilized and subsequently washed with deionized water for the removal of native oxides and dust particles after etching process in 2.0 M NaOH for 0.5 h at room temperature. The foil was then electro-polished at constant voltage of 12 V for 5 min in a mixture of CH_3CH_2OH: $HClO_4$ (4:1; % Vol). Polished Al foil was mounted in electrochemical cell which served as anode. Solution of H_2SO_4 and H_3PO_4 with equimolar ratio of 0.3 M was

* Corresponding author.
E-mail address: xfhan@iphy.ac.cn (X.F. Han).

http://dx.doi.org/10.1016/j.jmmm.2016.10.051
Received 8 September 2015; Received in revised form 5 October 2016; Accepted 9 October 2016
Available online 20 October 2016
0304-8853/

used for first anodization process carried out at 20 V for 5 h at 0 °C. Finally, nano-porous aluminum oxide was etched with H_3PO_4 (6 wt%) and Cr_2O_3 (2 wt%) inside furnace at 60 °C for 24 h. In order to remove concave ditches and keep the nano-porous hole open in Al foil, second step of anodization was carried out at similar conditions adopted during first process. Later on, one side of AAO template was Cu coated with thickness of 12 nm (NTs) and 200 nm (NWs) for conducting working electrode. Fe_3Pt NWs and NTs were electrodeposited at room temperature from an aqueous electrolyte consisting of 0.1 M $FeSO_4$, 0.012 M H_2PtCl_6 and 0.5 M Na_2SO_4. The pH value of solution was adjusted at 3 by adding diluted H_2SO_4. A conventional three electrode cell was used potentiostatically with Pt foil and saturated calomel electrode (SCE-KCl) were served as counter and reference electrode. Heat treatment effect in NWs and NTs was investigated with and without MF of 1 T at different temperatures for 1 h.

The microstructure of the samples was assessed by X-ray diffraction (XRD: RIGAKU-D/MAX-2400, Cu Kα, λ=0.154056 nm). The morphology of nanostructures was collected by field emission scanning electron microscopy (FE-SEM: Hitachi S-4800). Compositional analyses were performed with energy dispersive X-ray spectroscopy (EDS) integrated with FE-SEM. Magnetic properties were measured by vibrating sample magnetometer at room temperature (VSM: Microsense EV-9).

3. Results and discussion

Morphology of self-assembled AAO template with nano-channels of 200 nm was conducted with FE-SEM as shown in Fig. 1. The micrographs show highly homogeneous, clean and equispaced inter-pore distances. Etching parameters including etchant, temperature and time for template assisted NWs and NTs are highly important. The insets of Fig. 2 represent NWs and NTs after 1 h etching process with 1 M NaOH at room temperature. It can be observed that for morphology, room temperature etching is unable to remove template completely. Afterwards, the samples were etched with same etchant at 60 °C.

It can be seen that the unwanted template is completely removed after heat assisted etching process and left self-assembled NWs and NTs (main body of Fig. 2). Here, it is worth mentioning that etching process is highly important for Fe_3Pt NWs and NTs. Morphology predicts highly ordered, smooth and uniform NWs and NTs with average diameter of 200 nm which corresponds to average pore diameter of AAO templates. Average wall thickness and length of NTs are about 30 nm and 15 μm respectively, controlled by tuning the deposition rate.

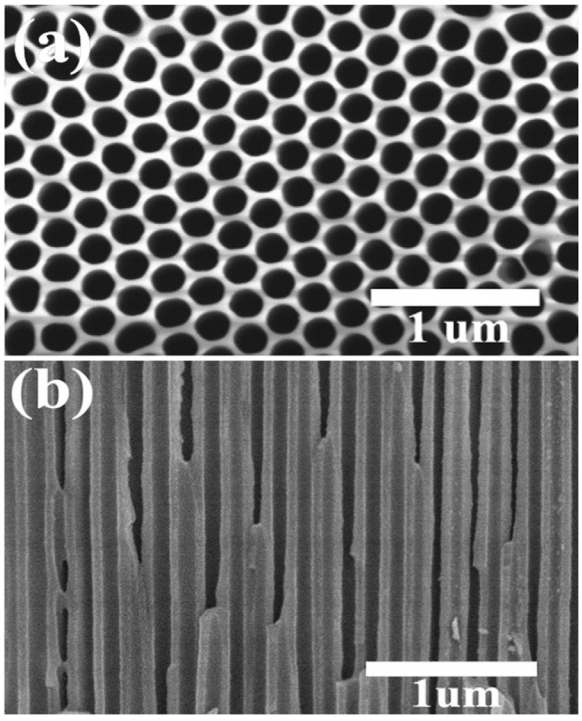

Fig. 1. Field emission scanning electron microscope (FE-SEM) images of AAO template (a) top surface, and (b) cross-sectional surface.

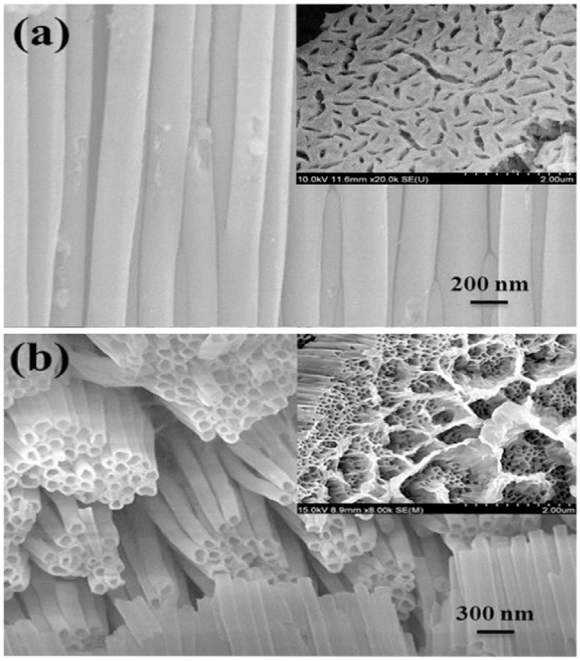

Fig. 2. FE-SEM micrographs of Fe_3Pt (a) NWs (b) NTs with average diameter of 200 nm after 1 h etching at 60 °C. The effect of room temperature etching on nanostructures with 1 M NaOH for 1 h is shown in the corresponding insets.

Room temperature XRD patterns of Fe_3Pt NWs and NTs with and without MF annealing are shown in Fig. 3. The peaks in all XRD patterns correspond to (111), (200), and (220) planes at all temperature ranges (400–700 °C). The lattice parameters of prepared samples were investigated by using the similar approach that was previously adopted by N. Adeela and her coworkers [28]. The numerical values for lattice parameters are 3.75 Å and 3.73 Å (JCPDS card no. 01-071-8364) for simple annealed (SA) and MF annealed Fe_3Pt NWs, respectively which are in good agreement with the value of 3.73 Å studied previously for bulk Fe_3Pt [29,30]. The chemically ordered face centered cubic (FCC) phase with Pm-3m space group of NWs is detected after heat treatment. In addition, crystallinity of the NWs is improved after simple annealing however this improvement is more effective for the case of MF annealing. In argument, most of the grains become aligned in the direction of easy axis of NWs due to the presence of external magnetic field (e.g. 1 T). Moreover, electrodeposited Fe_3Pt NTs showed amorphous behavior and heat treatment did not show any significant peak for both with and without MF annealing as shown in Fig. 4.

As-synthesized magnetic hysteresis loops measured for Fe_3Pt NWs and NTs are shown in Fig. 5. In 1D regime, especially for the case of Fe_3Pt, FePt, $FePt_3$ and CoPt alloys effective magnetic anisotropic field (H_k) plays a dominant role to understand easy axis of magnetization. Usually, there are three main contributions of H_k, shape anisotropic field, magnetostriction anisotropic field and magnetocrystalline anisotropic field. In case of NWs and NTs, shape anisotropy tends to align easy axis of magnetization parallel to applied magnetic field whereas magnetostriction anisotropy has opposite case. On the other hand, magnetocrystalline anisotropy is negligible due to polycrystalline (also shape anisotropy dominates in 1D structures) behavior of 1D electrodeposited nanostructure. In our case, easy direction of magnetization in Fe_3Pt NWs is parallel to NWs and NTs long axis due to shape

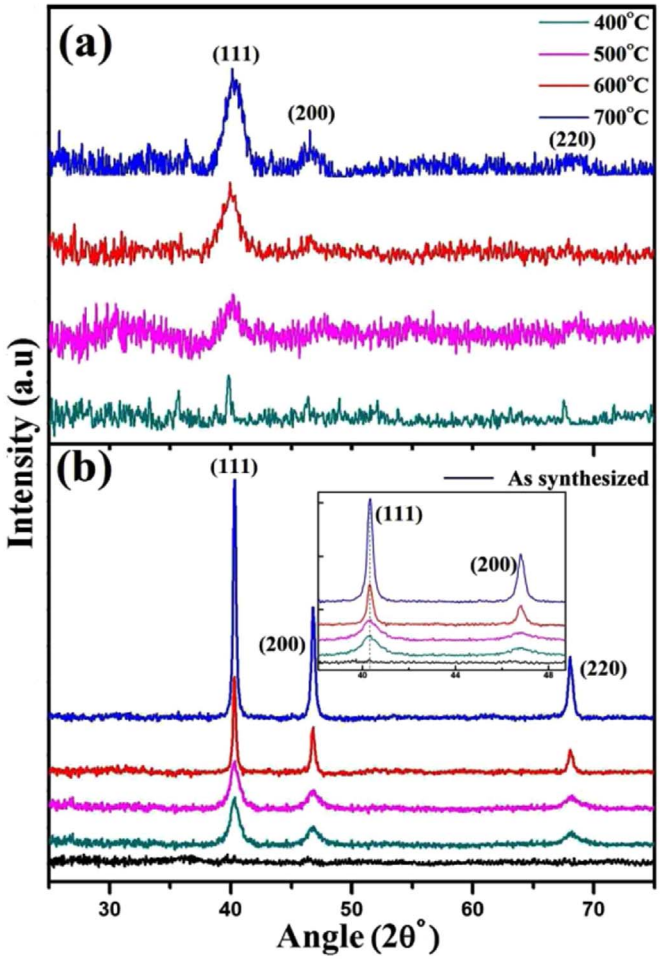

Fig. 3. XRD patterns of Fe_3Pt NWs embedded in AAO template after annealing at different temperatures, (a) without magnetic field, (b) with magnetic field of 1 T.

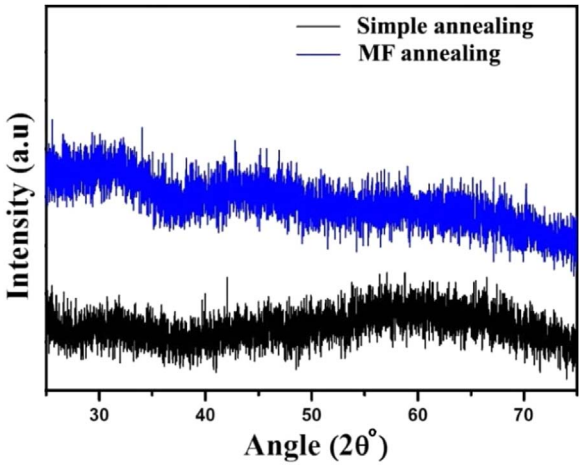

Fig. 4. XRD patterns of Fe_3Pt NTs embedded into AAO template after annealing at 700 °C, (a) without magnetic field, (b) with magnetic field of 1 T.

anisotropy.

Fig. 6 shows variation in magnetic coercivity (H_c) and squareness (SQ) in Fe_3Pt NWs as a function of annealing temperature with/without applied magnetic field of 1 T. It has been observed that H_c and SQ of NWs increase as a function of annealing temperature for both easy and hard axis of magnetization whereas, slight decrease in H_c has been observed in case of SA above 600 °C. The decrease in H_c is attributed to the strong interaction of (Al, $Fe)_2O_3$.

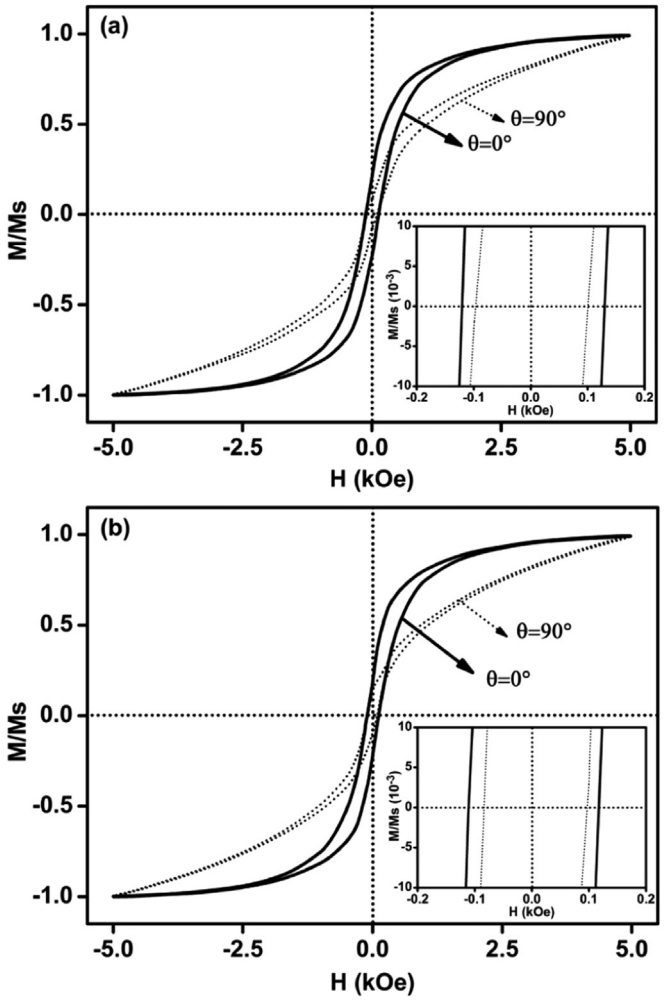

Fig. 5. As-synthesized hysteresis loops of (a) Fe_3Pt NWs (b) Fe_3Pt NTs, whereas solid and dotted lines show *M-H* loops in the field applied parallel and perpendicular to wire/tube long axis. Insets represent magnified view of their corresponding loops near the origin.

between Fe_3Pt NWs and AAO template which degrades overall magnetic properties of NWs. Magnetic coercive field has direct relation with saturation magnetization which can be written as

$$H_c \propto (\mathcal{U} + \mathcal{V} - w) M_s \quad (1)$$

where

$$\mathcal{U} = \frac{\pi (6M_n + 2L_n) a^2}{6b^2}$$

$$\mathcal{V} = 4\pi (N_\perp - N_\parallel)$$

$$w = 0.\ 7\pi a^2 b (4n + 1 - (-1)^n)/2D_i^3$$

and M_n and L_n are number of ellipsoids in wire, a is diameter of the NWs (length of short axis of the

ellipsoid), b is the distance between the centers of two ellipsoids (length of long axis of the ellipsoid), $N_\perp$ and $N_\parallel$ are demagnetization factors of the ellipsoid parallel and perpendicular to the NWs axis which depend on the aspect ratio of the ellipsoid and D_i is the interpore distance [31]. It can be seen in Eq. (1) that Hc increases due to increase in M_s depending on aspect ratio of wires and demagnetization factors. In case of Fe_3Pt NWs similar trend has been noticed as a function of annealing temperature whereas this trend is dominant for MF annealing when external magnetic field was applied parallel to NWs axis (Figs. 6(b) and 6(d)). In case of SA Bragg's peaks are not sharp and NWs have less value of H_c and SQ in comparison with MF annealing

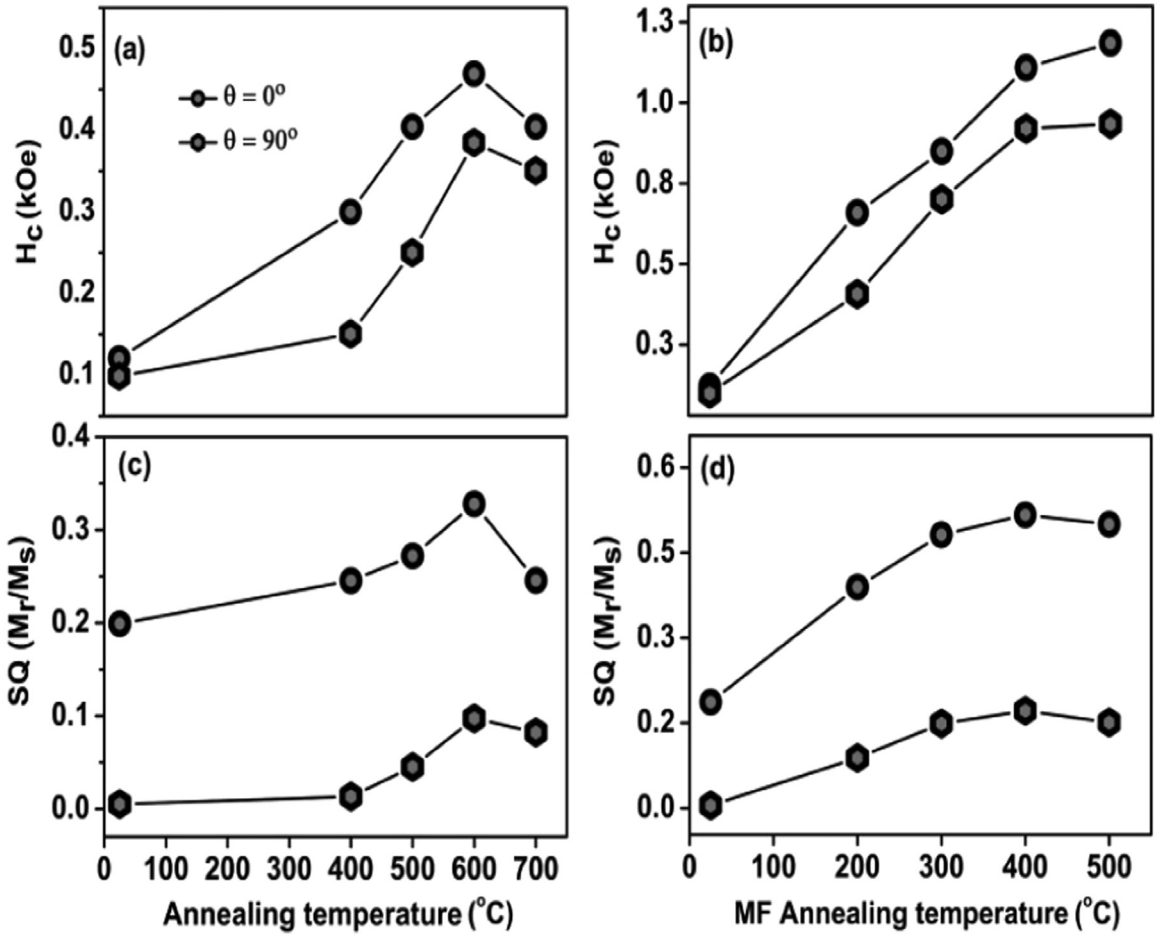

Fig. 6. Annealing temperature dependence of Hc and SQ in Fe_3Pt NWs: (a) Hc dependence on annealing temperature, (b) Hc dependence on MF annealing temperature, (c) SQ dependence on annealing temperature, and (d) SQ dependence on MF annealing temperature.

which can be seen in Figs. 6(a) and 6(c). This happens because MF annealing causes to relief stresses between neighboring grains and ordered atomic pairs of Fe and Pt contents suggested by XRD analyses which results in aligned free magnetic moments of Fe_3Pt nanostructure in the direction of external magnetic field. In addition, structural and magnetic properties of NWs correlate with each other. Both crystallinity and magnetic properties of Fe_3Pt NWs are improved as a function of annealing temperature under applied magnetic field of 1 T. A brief comparison of H_c and SQ due to annealing effect with and without.

magnetic field is mentioned in Table 1. Dependence of H_c and SQ in Fe_3Pt NTs as a function of annealing temperature with and without field of 1 T are shown in Fig. 7. It can be seen from Figs. 7(a) and 7(c) that initially there is slight increase in H_c and SQ due to SA which is due to the ferromagnetic nature of iron. But as the annealing temperature increases, fall in H_c and SQ values occur above 400 °C. The response of MF annealing is also observed for NTs when field was applied parallel and perpendicular to NTs long axis during MF annealing process (Figs. 7(b) and 7(d)). The effect of H_c for Fe_3Pt NTs is similar for both simple and MF annealing whereas SQ is larger for the case of MF annealing due to aligned magnetic moments in Fe_3Pt. Since in nanostructures, melting point is very less as compared to bulk alloys and metals therefore, in case of NT arrays, it could be easier to melt at high temperatures because the wall thickness is approximately 30 nm which is very small in comparison with NWs [32]. Reaction of FePt alloy with AAO template could possibly make oxides of Fe and Al and lead to the reduction in H_c and SQ. Similar annealing behavior has been reported for the case of CoPt where Co NWs were diffused with AAO templates which degrades overall magnetic properties [33]. The variations in the magnetic properties of Fe_3Pt NT arrays due to the effect of simple and MF annealing are shown in Table 2. It can be argued that magnetic field annealing and geometry of nanostructures drastically affect the structural and magnetic properties at nanoscale level.

Table 1
The variations in the magnetic properties of Fe_3Pt NW arrays due to the effect of simple and MF annealing.

Magnetic parameters	Fe_3Pt NWs		
	As deposited	SA at 600 °C	MF annealing at 500 °C
$H_{c\parallel}$ (Oe)	120.9	469.36	1200
$H_{c\perp}$ (Oe)	99	385.22	920
$SQ_{\parallel}$ (M_r/M_s)	0.199	0.33	0.55
$SQ_{\perp}$ (M_r/M_s)	0.05	0.10	0.15

4. Conclusions

Fe_3Pt NWs and NTs embedded in nano-porous alumina templates have been fabricated with dc electrodeposition process. Microstructural analyses show polycrystalline nature of NWs with FCC phase however heat treatment did not show any significant peak both with and without MF annealing. In both cases of simple and MF annealing, magnetic moments become parallel to wires long axis however the effect was dominant for MF annealing. The decrease in H_c and SQ for the Fe_3Pt NWs occurred at 600 °C as a result of simple annealing whereas H_c and SQ maintained its increasing trend in MF annealing. The situation is

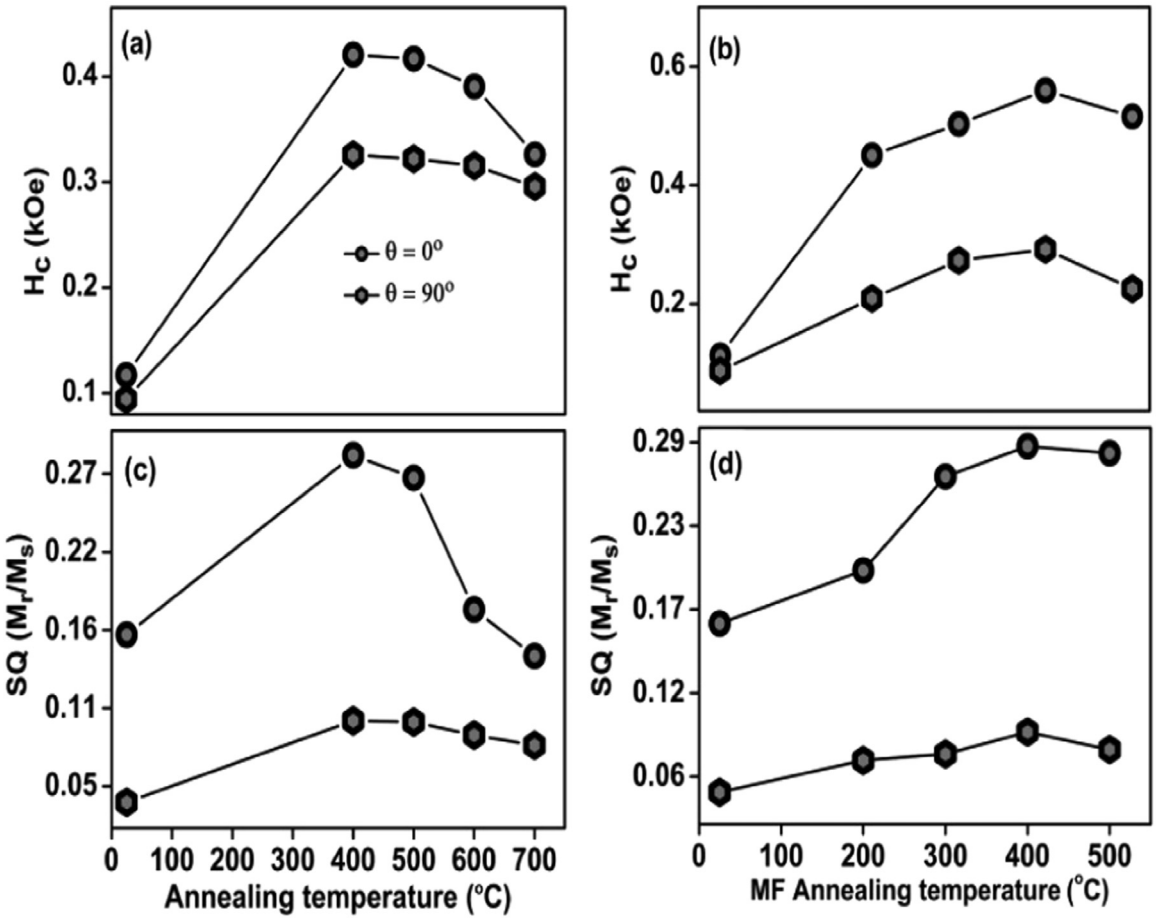

Fig. 7. Annealing temperature dependence of Hc and SQ in Fe_3Pt NTs: (a) Hc dependence on annealing temperature, (b) Hc dependence on MF annealing temperature, (c) SQ dependence on annealing temperature, and (d) SQ dependence on MF annealing temperature.

Table 2
The variations in the magnetic properties of Fe_3Pt NT arrays due to the effect of simple and MF annealing.

Magnetic parameters	Fe_3Pt NTs		
	As deposited	SA at 400 °C	MF annealing at 400 °C
$H_{c\parallel}$ (Oe)	115.2	411.63	560
$H_{c\perp}$ (Oe)	94.342	320.33	325
$SQ_{\parallel}$ (M_r/M_s)	0.16	0.26	0.28
$SQ_{\perp}$ (M_r/M_s)	0.04	0.08	0.09

different for Fe_3Pt NTs where both H_c and SQ were decreased at 400 °C. The decrease in magnetic properties is attributed to interaction of alumina templates with electrode-posited material. Therefore, it can be argued that magnetic field annealing and geometry of nanostructures affect the structural and magnetic properties at nanoscale level.

Acknowledgments

The project was supported by the State Key Project of Fundamental Research and 863 Plan Project of Ministry of Science and Technology [MOST, No. 2010CB934401 (Han-973 Project) and 2014AA032904 (Han-863 Project)], the National Natural Science Foundation of China [NSFC, Grant no. 11374351 (Han), 51229101 (X.-G. Zhang and Han), 11174341 (Wei- project), 11222432 (Wei- Young researcher project)], International collaborative research program between NSFC and ANR of France with foundation No. F040803, JSPS-NSFC joint project [11104338 (Liu DP)] and Russia-China joint project [MOST 2011DFR01060 (Han)].

References

[1] C. Morón, C. Cabrera, A. Morón, A. García, M. González, Sensors 15 (2015) 28340.
[2] H.W. Zhang, Y. Liu, S.H. Sun, Front. Phys. China 5 (2010) 347.
[3] Y. Huang, X.F. Duan, Y. Cui, C.M. Lieber, Nano Lett. (2) (2002) 101.
[4] M.H. Rehman, C.S. Liew, T.Y. Wah, J. Shuja, B. Daghighi, Sensors 15 (2015) 4430.
[5] P. Grunberg, Springer, 2009, pp. 661–683. http://dx.doi.org/10.1007/978-0-387-85600-1
[6] M.V. Kamalakar, A.K. Raychaudhuri, Phys. Rev. B. 82 (2010) 195425.
[7] J.E. Wegrowe, S.E. Gilbert, D. Kelly, B. Doudin, J.P. Ansermet, IEEE Trans. Magn. 34 (1998) 903.
[8] M.V. Kamalakar, A.K. Raychaudhuri, X.Y. Wei, J. Teng, P.D. Prewett, Appl. Phys. Lett. 95 (2009) 013112.
[9] J. Meier, B. Doudin, J.-Ph Ansermet, Appl. Phys. Lett. 79 (1996) 6010.
[10] U. Khan, M. Irfan, W.J. Li, N. Adeela, L. Pan, Q.T. Zhang, X.F. Han, Nanoscale 8 (2016) 14956.
[11] U. Khan, W.J. Li, N. Adeela, M. Irfan, K. Javed, C.H. Wan, S. Riaz, X.F. Han, Nanoscale 8 (2016) 6064.
[12] Z.Q. Jin, J. Li, N.N. Thadhani, Z.L. Wang, T. Vedantam, J.P. Liu, AIP Conf. Proc 845 (2006) 1157.
[13] J.H. Gao, Q.F. Zhan, W. He, D.L. Sun, Z.H. Cheng, Appl. Phys. Lett. 86 (2005) 232506.
[14] M. Sternik, S. Couet, J.L. Zewski, P.T. Jochym, K. Parlinski, A. Vantomme, K. Temst, P. Piekarz, J. Alloy. Comps 651 (2015) (528e536).
[15] L. Suber, P. Imperatori, E.M. Bauer, R. Porwal, D. Peddis, C. Cannas, A. Ardu, A. Mezzi, S. Kaciulis, A. Notargiacomo, L. Pilloni, J. Alloy. Compd. 663 (2016) 601.
[16] Y. Liu, Y. Jiang, X.L. Zhang, Y. Wang, Y.J. Zhang, H.L. Liu, H.J. Zhai, Y.Q. Liu, J.H. Yang, Y.S. Yan, J. Solid State Chem. 209 (2014) 69.
[17] C.L. Hua, Y.C. Zhou, L. Liao, R.L. Stamps, J. Magn. Magn. Mater. 386 (2015) 146.
[18] S. Muto, R. Oshima, F.E. Fujita, Metall. Trans. A 19A (1988) 2723.
[19] T. Kakeshita, T. Takeuchi, T. Fukuda, M. Tsujiguchi, T. Saburi, R. Oshima, S. Muto, Appl. Phys. Lett. 77 (2000) 1502.
[20] K. Javed, D.W. Shi, S.S. Ali, J. Jiang, P. Liu, X.F. Han, IEEE Trans. Magn. 50 (2014) 2301704.
[21] S.S. Ali, K. Javed, D.W. Shi, L.L. Tao, J. Jiang, G.J. Zhai, X.F. Han, J. Appl. Phys.

115 (2014) 17A762.
[22] N. Adeela, K. Maaz, U. Khan, S. Karim, M. Ahmad, M. Iqbal, S. Riaz, X.F. Han, M. Maqbool, Ceram. Int. 41 (2015) 12081.
[23] S.N. Hsiao, S.K. Chen, S.H. Liu, H.Y. Lee, J. Appl. Phys. 111 (2012) 07A313.
[24] K. Javed, W.J. Li, S.S. Ali, D.W. Shi, U. Khan, S. Riaz, X.F. Han, Sci. Rep. 5 (2015) 18203.
[25] M. Irfan, U. Khan, W.J. Li, N. Adeela, K. Javed, X.F. Han, Mater. Lett. 180 (2016) 235.
[26] M. Irfan, U. Khan, W.J. Li, W.J. Kong, K. Javed, X.F. Han, J. Alloy. Compd. 691 (2017) 1.
[27] M.I. Vázquez, V. Romero, V. Vega, J. García, V.M. Prida, B. Hernando, J. Benavente, Nanomaterials 5 (2015) 2192.
[28] N. Adeela, K. Maaz, U. Khan, S. Karim, A. Nisar, M. Ahmad, G. Ali, X.F. Han, J.L. Duan, J. Liu, J. Alloy. Comps 639 (2015) 533.
[29] H. Okamoto, ASM International, Materials Park, 1993, pp. 330–336.
[30] K.H.J. Buschow, P.G.V. Engen, R. Jongebreur, J. Magn. Magn. Mater. 38 (1) (1983).
[31] H.L. Su, G.B. Ji, S.L. Tang, Z. Li, B.X. Gu, Y.W. Du, Nanotechnology 16 (2005) 429.
[32] J. Wang, X. Chen, G. Wang, B. Wang, W. Lu, J. Zhao, Phys. Rev. B. 66 (2002) 085408.
[33] W. Li, Y. Peng, G.A. Jones, T.H. Shen, G. Hill, J. Appl. Phys. 7 (2005) 034308.